PNAS RESEARCH ARTICLE | GENETICS

Imprinted X chromosome inactivation in marsupials: The paternal X arrives at the egg with a silent DNA methylation profile

Ashley M. Milton[a], Laia Marín-Gual[b,c], Nicholas C. Lister[a], Kim L. McIntyre[a], Patrick G. S. Grady[d,e], Melanie K. Laird[f], Donna M. Bond[f], Timothy A. Hore[f], Rachel J. O'Neill[d,e], Andrew J. Pask[g], Marilyn B. Renfree[g], Aurora Ruiz-Herrera[b,c], and Paul D. Waters[a,1]

Affiliations are included on p. 5.

Edited by Marcus Feldman, Stanford University, Stanford, CA; received June 19, 2024; accepted July 22, 2024

X chromosome inactivation (XCI) is an epigenetic process that results in the transcriptional silencing of one X chromosome in the somatic cells of females. This phenomenon is common to both eutherian and marsupial mammals, but there are fundamental differences. In eutherians, the X chosen for silencing is random. DNA methylation on the eutherian inactive X is high at transcription start sites (TSSs) and their flanking regions, resulting in universally high DNA methylation. This contrasts XCI in marsupials where the paternally derived X is always silenced, and in which DNA methylation is low at TSSs and flanking regions. Here, we examined the DNA methylation status of the tammar wallaby X chromosome during spermatogenesis to determine the DNA methylation profile of the paternal X prior to and at fertilization. Whole genome enzymatic methylation sequencing was carried out on enriched flow-sorted populations of premeiotic, meiotic, and postmeiotic cells. We observed that the X displayed a pattern of DNA methylation from spermatogonia to mature sperm that reflected the inactive X in female somatic tissue. Therefore, the paternal X chromosome arrives at the egg with a DNA methylation profile that reflects the transcriptionally silent X in adult female somatic tissue. We present this epigenetic signature as a candidate for the long sought-after imprint for paternal XCI in marsupials.

DNA methylation | marsupial | imprinting | X chromosome inactivation | spermatogenesis

Significance

This research examines the contrasting mechanisms of eutherian and marsupial X chromosome inactivation (XCI) by investigating one of the key differences: paternal imprinting in marsupials. Analysis of DNA methylation patterns on the marsupial X chromosome during spermatogenesis revealed that genes on the paternal X chromosome exhibit a DNA methylation profile akin to the "silent" profile of genes on inactive X chromosomes in female somatic cells. This observation suggests a preexisting, silent DNA methylation landscape on the paternal X chromosome upon fertilization, which we hypothesize is the long sought-after imprint governing paternal XCI in marsupials.

Therian (eutherian and marsupial) mammals share an XX female: XY male sex chromosome system (reviewed in ref. 1) that evolved from a pair of autosomes in a therian ancestor. After recombination was suppressed between the pair, degeneration of the Y chromosome proceeded (2). Under classic theory (3), loss of gene function from the Y created a monosomy of the X in males, which resulted in pressure to transcriptionally up-regulate X borne genes, or at least a subset of haploinsufficient genes (4). This overexpression carried through to females, leading to the evolution of a mechanism to epigenetically silence one X chromosome in somatic cells, a process called X chromosome inactivation (XCI) (5).

In humans, one of the two X chromosomes is randomly chosen for silencing, and the long noncoding RNA (lncRNA) *XIST* is expressed from and coats the future inactive X (Xi) (6, 7). *XIST* RNA recruits epigenetic modifiers that deposit histone modifications typically associated with facultative heterochromatin, such as H3K27me3. Ultimately, DNA methylation (5mC) increases at transcription start sites (TSSs) to lock in the silent state (8, 9). In mice, the paternally derived X is initially silenced in the early blastocyst before it is reactivated in the embryo, in preparation for random XCI (10).

XCI also occurs in marsupials. Compared with eutherians (i.e., humans and mice), the Xi has a similar, but nonidentical, histone code that presumably results in its silencing (11, 12). Despite similarities in some of the repressive histone modifications (e.g., H3K27me3, H3K9me2) that accumulate on the Xi, there are fundamental differences in the XCI process between marsupials and eutherians. Marsupials do not have an *XIST* gene (13–16), rather they have an independently evolved lncRNA called *RSX*. Like *XIST*, *RSX* is expressed from and coats the future Xi (17). Marsupial XCI is paternally imprinted so that the X inherited from the father is silenced in all somatic cells of female offspring (18).

Another distinct XCI feature in marsupials is the global hypomethylation of the Xi compared to the active X (Xa) and the autosomes (19). This is accompanied by a DNA methylation profile that is low at (and flanking) the TSSs of genes on the Xi (20, 21). This contrasts the eutherian Xi, on which genes subject to silencing have high DNA methylation at their TSSs, which is also flanked by high DNA methylation levels. So despite differences in absolute DNA methylation levels across TSSs on the inactive X in eutherians and

Author contributions: A.R.-H. and P.D.W. designed research; A.M.M. and L.M.-G. performed research; M.B.R. contributed new reagents/analytic tools; A.M.M. and P.G.S.G. analyzed data; M.B.R. provided samples; A.M.M., L.M.-G., N.C.L., K.L.M., D.M.B., T.A.H., R.J.O., A.J.P., A.R.-H., and P.D.W. interpreted data; L.M.-G., N.C.L., K.L.M., P.G.S.G., M.K.L., D.M.B., T.A.H., R.J.O., A.J.P., M.B.R., and A.R.-H. commented on paper drafts; A.R.-H. and P.D.W. acquired funding; and A.M.M. and P.D.W. wrote the paper.

The authors declare no competing interest.

This article is a PNAS Direct Submission.

[1]To whom correspondence may be addressed. Email: p.waters@unsw.edu.au.

This article contains supporting information online at https://www.pnas.org/lookup/suppl/doi:10.1073/pnas.2412185121/-/DCSupplemental.

Published August 27, 2024.

marsupials, the DNA methylation landscape is uniform, which is consistent with genes that have reduced expression (22). Therefore, a flat DNA methylation profile was proposed to lock in the silent state of the marsupial Xi (20).

Importantly, DNA methylation is heritable through germ cells (egg and sperm), although it must be reset during germ cell development. There are two waves of global demethylation and remethylation during mammalian development: the first during gametogenesis and a second in early embryogenesis (23). Demethylation during gametogenesis is necessary to erase parent-specific imprinting in order to reset sex-specific imprinting marks (24) and maintain genomic integrity through transposon silencing (25). Early development demethylation, however, is necessary for acquisition of totipotency (26). Studies in mice have revealed that germ cell-specific DNA methylation marks are established after primordial germ cell (PGC) reprogramming. This can occur at different times and in different cellular environments in males and females (25, 27).

In mammals, the generation of sperm (spermatogenesis) is generally divided into three stages: i) proliferation and differentiation of spermatogonia (Spg); ii) meiosis, a reductional division, and iii) spermiogenesis, where round spermatids (RS) are transformed into densely compacted spermatozoa (mature sperm). Eutherians and marsupials appear to have commonalities in germline DNA methylation reprogramming, with relative timing of global methylation dynamics being shared in these two groups (28, 29). In the mouse, de novo methylation initiates as Spg proliferate (30). However, it is not known if this pattern is conserved in marsupials, or if autosomes and sex chromosomes are affected equally. This is relevant since mammalian sex chromosomes are characterized by meiotic-specific and highly dynamic epigenetic modifications.

During the first meiotic division, the X and Y form a transcriptionally silenced macrochromatin domain, called the sex body (31). This form of inactivation is called meiotic sex chromosome inactivation (MSCI) and is accompanied by the accumulation of repressive histone marks, including deacetylation of histones H3 and H4 and trimethylation of H3K9 (32–35). The transcriptional silencing of MSCI is also coupled with 3D higher-order chromatin remodeling (36), altogether necessary to maintain sex chromosome silencing in the male germ line. Whether this repressive pattern is also accompanied by changes in DNA methylation in marsupials needs further exploration.

Here, we examine the dynamics of DNA methylation on the paternally derived X chromosome before fertilization in a marsupial, the tammar wallaby (*Notamacropus eugenii*). We generated whole genome enzymatic methylation sequencing (EM-seq) from four populations of male germ cells: Spg, primary spermatocytes at pachytene/diplotene (P/D) stage, RS, and mature sperm. We show that at all stages the X chromosome has a DNA methylation profile across TSSs that is different to that of genes on autosomes. This DNA methylation profile mimics that of the Xi in female somatic tissue. Thus, we hypothesize that the whole X chromosome DNA methylation profile arriving at the egg at fertilization is the imprint that results in paternal XCI.

Results

We performed whole genome EM-seq on four pools of sorted tammar wallaby male germ cells: Spg, P/D, RS, and mature sperm (sperm) (Fig. 1 *A* and *B* and *SI Appendix*, Fig. S1 and Table S1). Two biological replicates were performed for each cell type, including 500 k and 630 k Spg (88.2% and 89.6% cell enrichment, respectively), 670 k and 760 k P/D cells (87.5% and 75.2% cell enrichment), 2 and 2.1 million RS (94.9% and 86.7% cell enrichment), and 890 k and 1 million spermatozoa (80.6% and 72.8% cell enrichment).

The resulting DNA methylation data were mapped to the tammar wallaby reference genome (37) with 60.8 to 75.0% efficiency (*SI Appendix*, Table S2). There was a bimodal distribution of DNA methylation levels (Fig. 1*C*). Global DNA methylation levels were similar between cell types, and there was no significant difference in median methylation percentage between the autosomes and X chromosome when data were processed in windows of 500 consecutive CpG sites (Fig. 1*D*).

We next performed a metagene analysis of TSSs of genes on the X chromosome and on the autosomes. In all four cell types, genes on autosomes had low DNA methylation at TSSs, which was flanked by high DNA methylation, a profile that is typical of transcriptionally active genes. This contrasted genes on the X, which had a flatter DNA methylation profile across TSSs, characteristic of transcriptionally silent genes (Fig. 1*E*). Strikingly, this profile (on what will be the paternally derived X after fertilization) resembled the DNA methylation landscape of the inactive X in female marsupial somatic cells (20), in which the paternal X is always silenced.

We generated single-locus plots for regions of interest and detected low DNA methylation levels at the *RSX* TSS in all cell types, flanked by high DNA methylation (Fig. 1*F*). This pattern is emblematic of transcriptionally active genes.

Discussion

Here, we characterized the dynamics of DNA methylation during spermatogenesis in a representative marsupial through EM-seq on four different male cell types. The observed bimodal distribution of DNA methylation levels (Fig. 1*C*) was expected as most CpGs are either close to fully methylated or unmethylated. Global DNA methylation levels did not appear to distinguish between autosomes and the future Xi at a whole chromosome level, as there were no significant differences detected in median methylation percentage (Fig. 1*D*).

A metagene TSS analysis was conducted because it was a more informative approach than calculating median methylation of whole chromosomes. Previous studies (20) have demonstrated that the DNA methylation landscape at the TSSs of genes is important for marsupial XCI. The resulting finding that X-linked genes had a "silent" DNA methylation profile across TSSs (in all cell types) (Fig. 1*E*) suggests that the X chromosome 5mC landscape must be established during early formation of the male germline prior to spermatogenesis, and this epigenetic signature persists to mature sperm. Further study is necessary to determine whether this pattern is established during PGC reprogramming.

It was previously proposed that imprinted XCI results from inheritance of the X chromosome, preinactivated by MSCI, from the paternal germline (38). Following prophase I, the X chromosome is persistently repressed in postmeiotic haploid cells forming postmeiotic sex chromatin (PSMC) in marsupials (39). However, it has been shown that MSCI-inactivated X genes are reactivated after meiosis, and then silenced once more (XCI) in the female offspring (40, 41). Based on the finding that the X is reactivated after MSCI, and our observation that a silent DNA methylation profile is established prior to MSCI, it is unlikely that MSCI establishes the imprint for XCI in marsupials.

Although the future Xi TSS DNA methylation landscape at fertilization mimics the DNA methylation profile in adult female somatic cells, the level of methylation is higher than expected. In adult somatic cells the inactive X is hypomethylated relative to the active X and the autosomes (19). This suggests that Xi

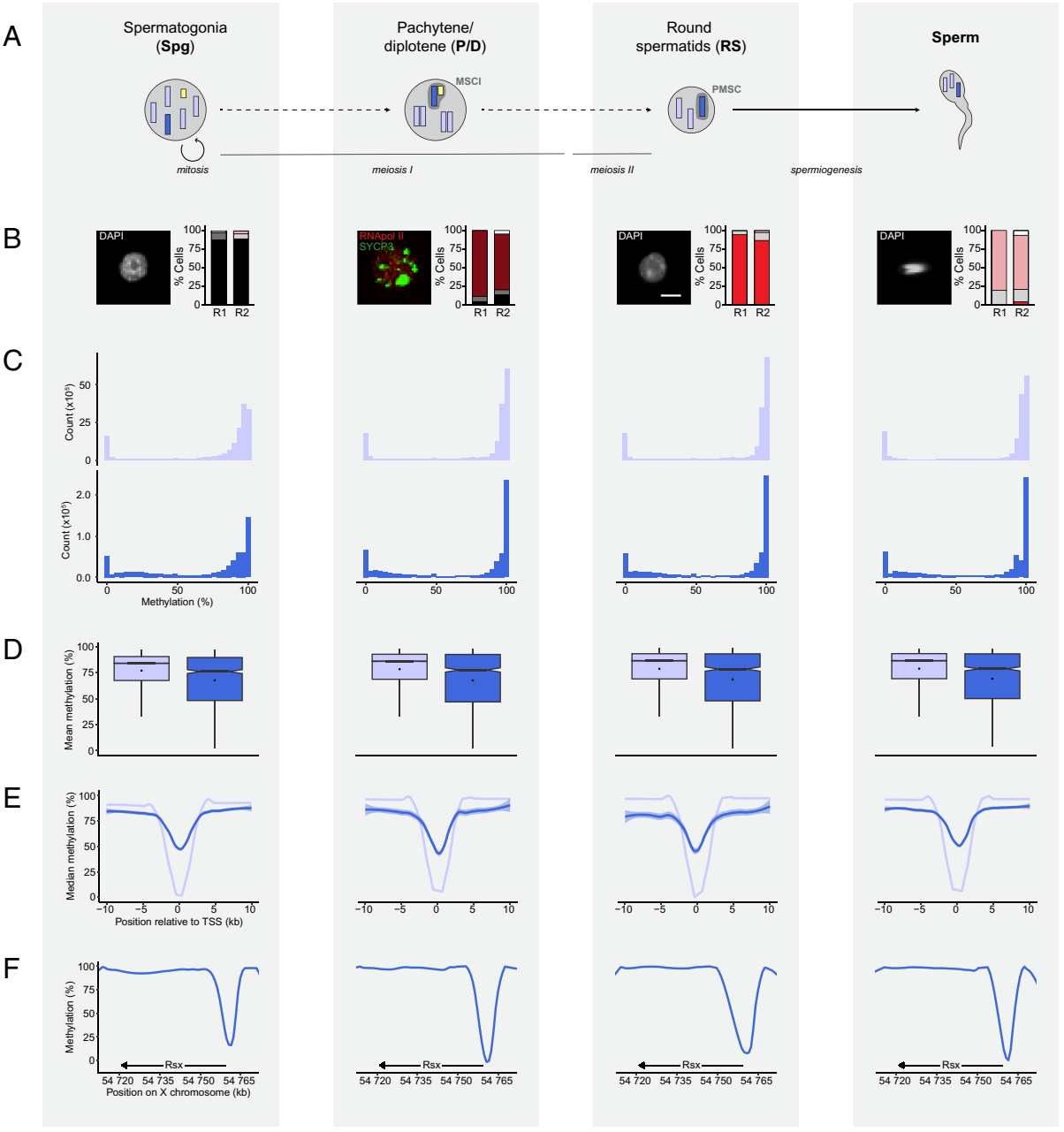

Fig. 1. Composition of cell categories and informative DNA methylation analyses for four different stages of marsupial spermatogenesis. (*A*) Schematic representation showing analyzed cell types, simplified chromosome pairing, MSCI, and PSMC dynamics during spermatogenesis progression. Each cell type—Spg, P/D, RS, mature sperm (Sperm)—represents a different stage of marsupial spermatogenesis. Note: Only one daughter cell is shown per cell division in this representation, and dashed arrows indicate instances where important spermatogenesis stages have been excluded for simplicity. See Fig. 2 for a more comprehensive depiction of spermatogenesis. (*B*) Tammar wallaby cell types used in EM-seq experiments. Two replicates (R1 and R2) were included per cell type. For each cell type, representative immunofluorescence images are shown. This includes labeling of specific meiotic proteins (SYCP3 in green and RNApol II in red) for primary spermatocytes and DAPI-stained DNA (grayscale) for other pre- and postmeiotic germ cells. (Scale bar: 10 μm.) Percentage of cell types from each flow-sorted population and each biological replicate are shown in column graphs. Cell type legend: Spg, leptotene/zygotene (L/Z), P/D, RS, elongating spermatids (ES). (*C*) Histograms of percent methylation at CpG sites. As expected, a bimodal distribution was observed for all cell types, in both autosomes (light blue) and X chromosome (dark blue). $N_{autosomes}$ = 15,975,551, N_{Xs} = 614,907. (*D*) DNA methylation data were filtered for coverage >14 in both biological replicates, and methylation levels were calculated for windows of 500 consecutive CpG sites without resampling. Boxplots represent autosomes (light blue) and X chromosome (dark blue) respectively, in each cell type. The central horizontal line represents the median of each group, and the dot represents the mean. $N_{autosomes}$ = 31959, N_{Xs} = 1230. (*E*) Metagene plots with smoothed line representation of median methylation at each position relative to the TSS ±10 kb. Autosomes (light blue) display a characteristic "active" U-shaped profile. X chromosomes (dark blue) have a typical "inactive" flatter profile. DNA methylation data were filtered for coverage >14 in both biological replicates, and each position relative to TSS had at least three data points. $N_{autosomes}$ = 20,001, $N_{Xs\text{-}Spg}$ = 7,635, $N_{Xs\text{-}P/D}$ = 3,289, $N_{Xs\text{-}RS}$ = 2,525, $N_{Xs\text{-}Sperm}$ = 10,097. (*F*) Smoothed line representation of median methylation at the *RSX* locus. For each cell type, there is a typical "active" U-shaped profile at the *RSX* TSS. DNA methylation data were filtered for coverage >9 in both biological replicates. N_{Spg} = 307, $N_{P/D}$ = 254, N_{RS} = 246, N_{Sperm} = 311.

methylation levels must be reduced at a stage prior to the development of adult somatic cells. The simplest explanation for diluting DNA methylation on the Xi (and maintaining a flat profile across TSSs) in the somatic cells of adult females is passive DNA demethylation during early somatic cell divisions.

We focused on *RSX*, the marsupial-specific lncRNA with *Xist*-like properties that is expressed from the Xi during marsupial XCI (17, 42). Notably, we detected low DNA methylation levels at the *RSX* TSS in all cell types, surrounded by high DNA methylation (Fig. 1*F*), a common pattern of transcriptionally

active genes. This observation suggests that this essential lncRNA escapes silencing during spermatogenesis. Moreover, our results align with *RSX* being expressed from the earliest embryonic stages (E3.5) and restricted to the paternal X chromosome, supporting that XCI occurs rapidly after embryonic genome activation (41).

Our metagene analyses suggest that on the marsupial Xi, most genes have an inactive flat DNA methylation profile at their TSS prior to spermatogenesis (Fig. 1*E*). Those genes that do escape silencing may possess an active DNA methylation profile (such as that of *RSX*, Fig. 1*F*). In light of our results, we hypothesize that this chromosome-wide pattern of TSS DNA methylation is part of the epigenetic imprint that primes the paternal X chromosome for inactivation.

With the paternal X already possessing a silent DNA methylation pattern prior to fertilization (Fig. 2), there must be subsequent recruitment of inactive histone modifications to reinforce the silent state of the Xi during this process (11, 12, 42). This contrasts the eutherian system, in which histone modifications occur in the blastocyst (10), and the DNA methylation landscape is established later in development, locking in the inactive state of the Xi (43).

It should be noted that this study has limitations owing to the species examined. The tammar wallaby is a wild Australian animal. Being a nonstandard model organism, there is no capacity to establish a knockout wallaby to demonstrate that perturbing DNA methylation on the future Xi would wipe the XCI imprint. Additionally, there is no meiotic cell culture model available for experimental manipulation. This study did not examine embryos, on account of wallabies being wild animals that produce just one embryo per female per year—and the female must be killed to obtain the embryo. Finally, expanding analysis to additional species requires a further model species with relatively large testes in order to obtain sufficient material for fluorescence-activated cell sorting (FACS) and EM-seq. This excludes smaller, more practical model species such as "marsupial mice" (e.g., *Sminthopsis* spp).

Overall, our results in tammar wallaby provide insight into the decades-old question surrounding the epigenetic mechanisms responsible for imprinted XCI in marsupials. Metagene analyses using whole genome methylation sequencing during marsupial spermatogenesis show that the DNA methylation landscape is established before the onset of meiosis and that the paternal X arrives at the egg with a transcriptionally silent DNA methylation profile, a unique finding for mammals.

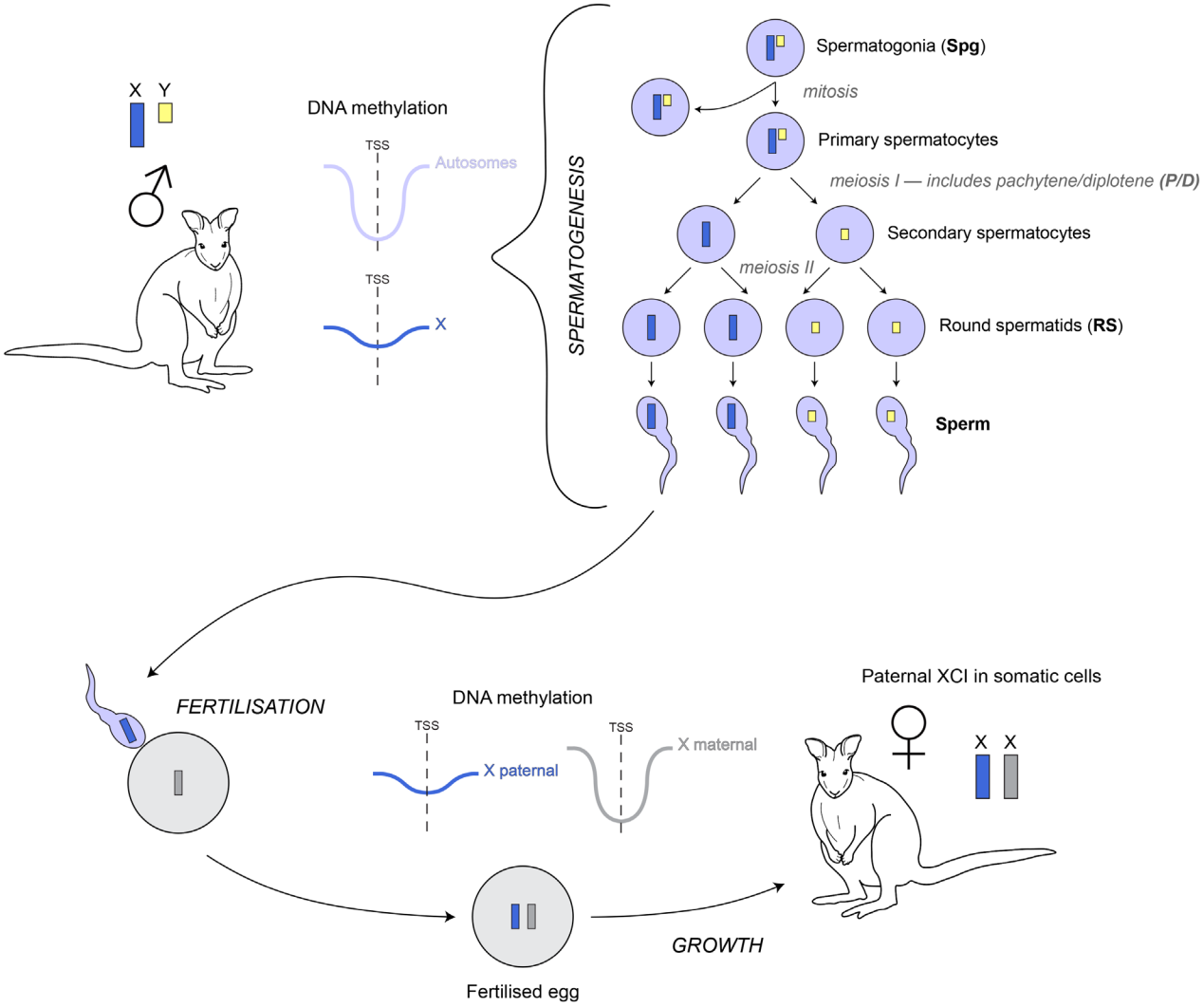

Fig. 2. Proposed model for the epigenetic imprint that results in paternal XCI in marsupials. Within each of the four male tammar wallaby cell types, there was a different DNA methylation profile across TSSs between the autosomes (light blue) and the X chromosome (dark blue). In each of the four cell types—Spg, P/D, RS, sperm—there was a flat DNA methylation profile throughout spermatogenesis across TSSs on the X chromosome, which will be the paternal X chromosome after fertilization. The paternal X chromosome therefore bears a DNA methylation signature (prior to fertilization) that reflects the inactive X in female somatic tissue. We hypothesize that this profile is distinct from maternal at the time of fertilization and is the imprint that results in paternal XCI.

Materials and Methods

Biological Samples. Tammar wallaby males (N = 2, *N. eugenii*) were collected from wild populations originating on Kangaroo Island (South Australia) that were held in a breeding colony in Melbourne (Victoria, Australia). Animals were held and tissues collected under approval by the Animal Ethics Committee (University of Melbourne).

FACS. Testis disaggregation and flow sorting of germ cells were performed as previously described (36, 44). Briefly, decapsulated testis were mechanically disaggregated and incubated in GBSS with collagenase type II (0.5 mg/mL) and Dnase I (1 μg/mL) at 33 °C for 30 min with agitation. Subsequently, trypsin (0.37 mg/mL) was added, incubated at 33 °C for 30 min and finally inactivated with fetal bovine serum. Germ cells at a concentration of 1 million cells/mL were incubated in formaldehyde (1%) for 10 min prior to FACS. Glycine (0.125 M) was added and incubated with agitation at room temperature for 5 min and then at 4 °C for 15 min. Cells were then centrifuged for 10 min at 720 × g at 4 °C and resuspended in 1 × PBS with Hoechst 33342 staining. Germ cells were sorted using a BD InfluxTM (BD Biosciences) coupled with an ultraviolet laser (355 nm). Four cell populations were isolated by plotting Hoechst Blue (UV355–460/50) vs. Hoechst red (UV355–670/30) emissions to discriminate cells by both their DNA content and their complexity: Spg (2n, 2c), primary spermatocytes (2n, 4c), RS (n, 1c), and sperm (n, 1c).

Cell enrichment of each flow-sorted population was evaluated by immunofluorescence using specific meiotic proteins and DAPI morphology. Briefly, cells were permeabilized with 0.05% Triton X-100 diluted in PBS at 37 °C for 10 min. Primary and secondary (all from Jackson ImmunoResearch) antibodies were then incubated overnight at 4 °C and 35 min at 37 °C, respectively. Cells were fixed on slides and then mounted with DAPI diluted in Vectashield (Vector Laboratories).

Primary spermatocytes were identified based on SYCP3 (abcam, ab15093, dilution 1:100) and RNA polymerase II (abcam, ab5408, dilution 1:200) patterns. Cell enrichment of Spg, RS, and sperm was determined based on nucleus morphology and DAPI pattern. Slides were analyzed using fluorescence microscopy (Axiophot, Zeiss) coupled with a ProgRes® CS10plus, Jenoptik camera. Representative images were captured with ACO XY (A. Coloma, Open Microscopy). Between 80 and 100 cells were counted for each flow-sorted population and only populations with a cell enrichment higher than 70% were considered for subsequent experiments.

Whole Genome EM-seq. Each flow-sorted population was incubated in lysis buffer containing 0.1 mg/mL proteinase K at 65 °C to extract genomic DNA. After 2 h, 0.3 mg/mL RNAse A was added and incubated for 1 h at 37 °C. DNA was then purified with phenol:chloroform and precipitated overnight in isopropanol at −20 °C. Genomic DNA was centrifuged at 13,000 × g for 30 min at 4 °C, washed with 70% ethanol, air dried at room temperature, and finally resuspended in Mili-Q water. DNA concentration and quality were checked on a Qubit and Agilent Bioanalyzer System, respectively, prior to sequencing. Library preparation and subsequent whole-genome EM-seq using Illumina NovaSeq 6000 (2 × 150 bp, >90 Gb, 30× coverage) were performed by CNAG (Centro Nacional de Análisis Genómico, Spain). The resulting raw sequence data are available on the NCBI Sequence Read Archive as part of BioProject PRJNA1051171 (45).

EM-seq Data Processing. All raw reads were trimmed using Trimmomatic (46) (version 0.38) with a head crop of 10, sliding window of 5:15, and minimum length of 30. Bismark (47) Genome Preparation (bismark version 0.22.3) was run to generate the requisite files for the Bismark Genome Alignment. Bowtie (48) version 2.3.5.1 and perl version 5.28.0 were used. The trimmed reads were then aligned to the reference genome (37) using Bismark Genome Alignment with a –score_min of L,0, -0.6. Hisat2 version 2.1.0 and samtools (49) version 1.13 were used. Bam files were deduplicated with Bismark Deduplicate and CpG reports were generated using Bismark Methylation Extractor.

EM-seq Data Analysis and Visualization. Once the CpG reports were obtained, the function methRead from the R package methyKit (50) was used to import the files with a minimum coverage of 1, and normalizeCoverage was used to normalize coverage between the different samples. Samples were united and destranded using unite. Percent methylation was calculated for each position using percMethylation.

Next, the percent methylation dataframe was intersected with a dataframe containing start and end positions for windows 10 kb either side of TSSs of annotated genes in the tammar wallaby genome. CpG positions that fell within a window were retained. The position of each CpG relative to the TSS was calculated. Custom scripts were used to generate plots, including coverage histograms, DNA methylation histograms, histograms of CpG count relative to TSS, boxplots of mean CpG % methylation, smoothed line plots representing median methylation level relative to TSS and plots representing methylation levels around the *RSX* locus. See GitHub for details (https://github.com/Ashley-Milton/MEU-meiosis-meth/). In order to generate the *RSX* methylation plots, the NCBI genome browser was used to download the *RSX* sequence from the mMonDom1.pri (*Monodelphis domestica*) genome. This sequence was BLASTed against the tammar wallaby reference genome (with default settings and a tabular output style) to determine the position of *RSX*. The BLAST output table was filtered for results on only the X chromosome, with a length of at least 100 bp.

Data, Materials, and Software Availability. Raw EM-seq data have been deposited in NCBI Sequence Read Archive (PRJNA1051171) (45). Tammar wallaby reference genome data can be accessed in the NCBI Sequence Read Archive (PRJNA956953) (37).

ACKNOWLEDGMENTS. P.D.W. is supported by Australian Research Council Discovery Projects (DP210103512 and DP220101429) and by a National Health and Medical Research Council Ideas Grant (2021172). A.R.-H. acknowledges the Spanish Ministry of Science and Innovation (PID2020-112557 GB-I00) and the Agència de Gestió d'Ajuts Universitaris i de Recerca, AGAUR (2021SGR00122) and the Catalan Institution for Research and Advanced Studies (ICREA). A.M.M. and K.L.M are supported by Australian Government Research Training Program Scholarships. L.M.-G. was supported by an FPU predoctoral fellowship from the Spanish Ministry of Science, Innovation and University (FPU18/03867 and EST22/00661).

Author affiliations: [a]School of Biotechnology and Biomolecular Sciences, Faculty of Science, The University of New South Wales, Sydney, NSW 2052, Australia; [b]Departament de Biologia Cellular, Fisiologia i Immunologia, Universitat Autònoma de Barcelona, Cerdanyola del Vallès 08193, Spain; [c]Genome Integrity and Instability Group, Institut de Biotecnologia i Biomedicina, Universitat Autònoma de Barcelona, Cerdanyola del Vallès 08193, Spain; [d]Department of Molecular and Cell Biology, University of Connecticut, Storrs, CT 06269; [e]Institute for Systems Genomics, University of Connecticut, Storrs, CT 06269; [f]Department of Anatomy, University of Otago, Dunedin 9016, New Zealand; and [g]School of BioSciences, The University of Melbourne, Parkville, VIC 3010, Australia

1. J. A. Graves, The evolution of mammalian sex chromosomes and the origin of sex determining genes. *Philos. Trans. R. Soc. Lond. B Biol. Sci.* **350**, 305–311; discussion 311–302 (1995).
2. B. Charlesworth, The evolution of sex chromosomes. *Science* **251**, 1030–1033 (1991).
3. S. Ohno, *Sex Chromosomes and Sex-Linked Genes, Monographs on Endocrinology* (Springer-Verlag, ed. 1, 1967), p. 192, 10.1007/978-3-642-88178-7.
4. F. Lin, K. Xing, J. Zhang, X. He, Expression reduction in mammalian X chromosome evolution refutes Ohno's hypothesis of dosage compensation. *Proc. Natl. Acad. Sci. U.S.A.* **109**, 11752–11757 (2012).
5. M. F. Lyon, Gene action in the X-chromosome of the mouse (Mus musculus L.). *Nature* **190**, 372–373 (1961).
6. C. J. Brown *et al.*, A gene from the region of the human X inactivation centre is expressed exclusively from the inactive X chromosome. *Nature* **349**, 38–44 (1991).
7. C. M. Clemson, J. A. McNeil, H. F. Willard, J. B. Lawrence, XIST RNA paints the inactive X chromosome at interphase: Evidence for a novel RNA involved in nuclear/chromosome structure. *J. Cell Biol.* **132**, 259–275 (1996).
8. D. P. Norris, N. Brockdorff, S. Rastan, Methylation status of CpG-rich islands on active and inactive mouse X chromosomes. *Mamm. Genome* **1**, 78–83 (1991).
9. C. Tribioli *et al.*, Methylation and sequence analysis around EagI sites: Identification of 28 new CpG islands in XQ24-XQ28. *Nucleic Acids Res.* **20**, 727–733 (1992).
10. I. Okamoto *et al.*, Eutherian mammals use diverse strategies to initiate X-chromosome inactivation during development. *Nature* **472**, 370–374 (2011).
11. W. Rens, M. S. Wallduck, F. L. Lovell, M. A. Ferguson-Smith, A. C. Ferguson-Smith, Epigenetic modifications on X chromosomes in marsupial and monotreme mammals and implications for evolution of dosage compensation. *Proc. Natl. Acad. Sci. U.S.A.* **107**, 17657–17662 (2010).
12. J. Chaumeil *et al.*, Evolution from XIST-independent to XIST-controlled X-chromosome inactivation: Epigenetic modifications in distantly related mammals. *PLoS One* **6**, e19040 (2011).
13. L. S. Davidow *et al.*, The search for a marsupial XIC reveals a break with vertebrate synteny. *Chromosome Res.* **15**, 137–146 (2007).
14. L. Duret, C. Chureau, S. Samain, J. Weissenbach, P. Avner, The Xist RNA gene evolved in eutherians by pseudogenization of a protein-coding gene. *Science* **312**, 1653–1655 (2006).
15. T. Hore, E. Koina, M. Wakefield, J. Graves, The region homologous to the X-chromosome inactivation centre has been disrupted in marsupial and monotreme mammals. *Chromosome Res.* **15**, 147–161 (2007).

16. A. I. Shevchenko *et al.*, Genes flanking Xist in mouse and human are separated on the X chromosome in American marsupials. *Chromosome Res.* **15**, 127–136 (2007).
17. J. Grant *et al.*, Rsx is a metatherian RNA with Xist-like properties in X-chromosome inactivation. *Nature* **487**, 254–258 (2012).
18. D. W. Cooper, P. G. Johnston, J. M. Watson, J. A. M. Graves, X-inactivation in marsupials and monotremes. *Semin. Dev. Biol.* **4**, 117–128 (1993).
19. E. D. Ingles, J. E. Deakin, Global DNA methylation patterns on marsupial and devil facial tumour chromosomes. *Mol. Cytogenet.* **8**, 74 (2015).
20. S. A. Waters *et al.*, Landscape of DNA methylation on the marsupial X. *Mol. Biol. Evol.* **35**, 431–439 (2018).
21. D. Singh *et al.*, Koala methylomes reveal divergent and conserved DNA methylation signatures of X chromosome regulation. *Proc. Biol. Sci.* **288**, 20202244 (2021).
22. C. A. Kapourani, G. Sanguinetti, Higher order methylation features for clustering and prediction in epigenomic studies. *Bioinformatics* **32**, i405–i412 (2016).
23. D. M. Messerschmidt, B. B. Knowles, D. Solter, DNA methylation dynamics during epigenetic reprogramming in the germline and preimplantation embryos. *Genes Dev.* **28**, 812–828 (2014).
24. M. S. Bartolomei, A. C. Ferguson-Smith, Mammalian genomic imprinting. *Cold Spring Harb. Perspect. Biol.* **3**, a002592 (2011).
25. H. Sasaki, Y. Matsui, Epigenetic events in mammalian germ-cell development: Reprogramming and beyond. *Nat. Rev. Genet.* **9**, 129–140 (2008).
26. M. A. Surani, Imprinting and the initiation of gene silencing in the germ line. *Cell* **93**, 309–312 (1998).
27. M. Saitou, M. Yamaji, Primordial germ cells in mice. *Cold Spring Harb. Perspect. Biol.* **4**, a008375 (2012).
28. T. Ishihara, D. Hickford, G. Shaw, A. J. Pask, M. B. Renfree, DNA methylation dynamics in the germline of the marsupial tammar wallaby, *Macropus eugenii*. *DNA Res.* **26**, 85–94 (2019).
29. D. M. Bond *et al.*, The admixed brushtail possum genome reveals invasion history in New Zealand and novel imprinted genes. *Nat. Commun.* **14**, 6364 (2023).
30. S. K. Kota, R. Feil, Epigenetic transitions in germ cell development and meiosis. *Dev. Cell* **19**, 675–686 (2010).
31. T. Wiltshire, C. Park, M. A. Handel, Chromatin configuration during meiosis I prophase of spermatogenesis. *Mol. Reprod. Dev.* **49**, 70–80 (1998).
32. M. A. Handel, The XY body: A specialized meiotic chromatin domain. *Exp. Cell Res.* **296**, 57–63 (2004).
33. C. Richler, H. Soreq, J. Wahrman, X inactivation in mammalian testis is correlated with inactive X-specific transcription. *Nat. Genet.* **2**, 192–195 (1992).
34. J. M. Turner *et al.*, Silencing of unsynapsed meiotic chromosomes in the mouse. *Nat. Genet.* **37**, 41–47 (2005).
35. P. D. Waters, A. Ruiz-Herrera, Meiotic executioner genes protect the Y From extinction. *Trends Genet.* **36**, 728–738 (2020).
36. C. Vara *et al.*, Three-dimensional genomic structure and cohesin occupancy correlate with transcriptional activity during spermatogenesis. *Cell Rep.* **28**, 352–367.e9 (2019).
37. P. G. S. Grady, R. J. O'Neill, Tammar wallaby (*M. eugenii*) T2T genome. NCBI SRA. https://www.ncbi.nlm.nih.gov/bioproject/PRJNA956953/. Deposited 18 April 2023.
38. K. D. Huynh, J. T. Lee, Inheritance of a pre-inactivated paternal X chromosome in early mouse embryos. *Nature* **426**, 857–862 (2003).
39. S. H. Namekawa, J. L. VandeBerg, J. R. McCarrey, J. T. Lee, Sex chromosome silencing in the marsupial male germ line. *Proc. Natl. Acad. Sci. U.S.A.* **104**, 9730–9735 (2007).
40. S. K. Mahadevaiah *et al.*, Key features of the X inactivation process are conserved between marsupials and eutherians. *Curr. Biol.* **19**, 1478–1484 (2009).
41. S. K. Mahadevaiah, M. N. Sangrithi, T. Hirota, J. M. A. Turner, A single-cell transcriptome atlas of marsupial embryogenesis and X inactivation. *Nature* **586**, 612–617 (2020).
42. X. Wang, K. C. Douglas, J. L. Vandeberg, A. G. Clark, P. B. Samollow, Chromosome-wide profiling of X-chromosome inactivation and epigenetic states in fetal brain and placenta of the opossum, Monodelphis domestica. *Genome Res.* **24**, 70–83 (2014).
43. L. F. Lock, N. Takagi, G. R. Martin, Methylation of the Hprt gene on the inactive X occurs after chromosome inactivation. *Cell* **48**, 39–46 (1987).
44. C. Vara *et al.*, The impact of chromosomal fusions on 3D genome folding and recombination in the germ line. *Nat. Commun.* **12**, 2981 (2021).
45. A. M. Milton, L. Marín-Gual, A. Ruiz-Herrera, P. D. Waters, *Notamacropus eugenii* raw sequence reads. NCBI SRA. https://www.ncbi.nlm.nih.gov/bioproject/PRJNA1051171. Deposited 29 January 2024.
46. A. M. Bolger, M. Lohse, B. Usadel, Trimmomatic: A flexible trimmer for Illumina sequence data. *Bioinformatics* **30**, 2114–2120 (2014).
47. F. Krueger, S. R. Andrews, Bismark: A flexible aligner and methylation caller for Bisulfite-Seq applications. *Bioinformatics* **27**, 1571–1572 (2011).
48. B. Langmead, S. L. Salzberg, Fast gapped-read alignment with Bowtie 2. *Nat. Methods* **9**, 357–359 (2012).
49. P. Danecek *et al.*, Twelve years of SAMtools and BCFtools. *Gigascience* **10**, giab008 (2021).
50. A. Akalin *et al.*, methylKit: A comprehensive R package for the analysis of genome-wide DNA methylation profiles. *Genome Biol.* **13**, R87 (2012).